

Nanostructured interfaces in polymer solar cells

W. Wiedemann,¹ L. Sims,¹ A. Abdellah,² A. Exner,² R. Meier,³ K. P. Musselman,⁴
J. L. MacManus-Driscoll,⁴ P. Müller-Buschbaum,³ G. Scarpa,² P. Lugli,² and
L. Schmidt-Mende^{1,a)}

¹Department of Physics, Center for NanoScience (CeNS), Ludwig-Maximilians University, Amalienstr. 54, 80799 Munich, Germany

²Institute for Nanoelectronics, Technische Universität München, Theresienstr. 90, 80333 München, Germany

³Physik-Department, Technische Universität München, LS E13, James-Frank-Str. 1, 85747 Garching, Germany

⁴Department of Materials Science and Metallurgy, University of Cambridge, Pembroke Street, CB2 3QZ Cambridge, United Kingdom

(Received 26 February 2010; accepted 9 June 2010; published online 30 June 2010)

The morphology in organic photovoltaics plays a key role in determining the device efficiency. We propose a method to fabricate bilayer devices with controlled nanostructured interfaces by combining nanoimprinting and lamination techniques. This technique allows us to achieve a network structure of donor-acceptor material with a ~ 80 nm periodicity and ~ 40 nm width. These structures have an abrupt interface between the donor and acceptor materials and show an increased effective interfacial area and photovoltaic performance compared to bilayer solar cells. In contrast to blend films, they will allow an in depth analysis of the influence of morphology on interfacial physical processes. © 2010 American Institute of Physics. [doi:10.1063/1.3458809]

Since the initial solution processed bulk heterojunction solar cells,^{1,2} significant progress has been made in this field reaching efficiencies over 6%.³ The use of organic solar cells offers a number of advantages over inorganic alternatives, such as mechanical flexibility, transparency, and easy production.⁴ However, in terms of stability and efficiency, it is very important to make further improvements to organic cells, in order for them to be competitive to inorganic devices. Therefore, a deeper understanding of the physical processes taking place in organic solar cells is of crucial importance. The interfaces in organic bulk heterojunction solar cells (BHJ) are not well defined and prohibit an analysis of the interfacial physics in detail. In contrast to the BHJ, for which two organic materials are spin coated from a blend solution on top of the electrode, a bilayer (BL) approach gives a well-defined structure that allows considerable insight into the device physics.^{5,6}

In this work, the focus is on different device structures consisting of poly(3-hexylthiophene) (P3HT) and [6,6]-phenyl-C61-butyric acid methyl ester (PCBM). The first structure is a BL cell [Fig. 1(a)], a second is called a stratified BL (SBL), where the PCBM layer has been spin coated on top of the P3HT layer [Fig. 1(b)], while using an orthogonal solvent combination in the P3HT and PCBM solutions. The third one is a nanostructured BL (NBL) device where the P3HT was nanoimprinted via nanoimprint lithography (NIL) using an anodic aluminum oxide (AAO) working as a stamp [Fig. 1(c)]. For BL and NBL cells, the second organic layer, PCBM, was deposited via a lift-off lamination technique.⁷ The lamination technique allows the addition of a second layer to fabricate BL cells with controlled and precisely designed interfaces, minimizing alteration of the first layer.

Solar cells are prepared by first spin coating (30 s at 5000 rpm) an electron blocking layer of PEDOT:PSS (H. C.

Starck) on cleaned ITO substrates (Solems, ITO thickness approximately 125 nm, sheet resistance approximately 50 Ω /sq). The P3HT (Merck, 28 mg/ml in chlorobenzene) was spin coated (30 s at 2000 rpm) on top of the substrate. Imprinting was performed with a state-of-the-art NIL tool [Obducat 2.5" equipment, Obducat, Sweden (Ref. 8)] at

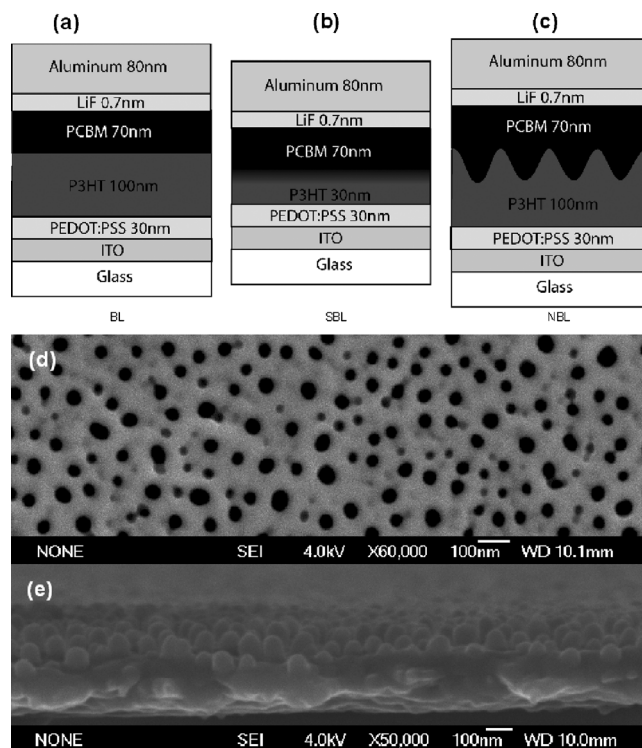


FIG. 1. Schematics of the different structures compared in this study: (a) a BL cell structure with a flat and abrupt interface, (b) a SBL structure with a certain degree of intermixing at the interface, and (c) a NBL cell with abrupt nanostructured interface between the donor and acceptor layers. In (d) the anodized alumina membrane used as a stamp for the imprinting process, and (e) a cross section SEM picture of the imprinted P3HT nanostructure.

^{a)}Electronic mail: l.schmidt-mende@lmu.de.

125 °C with an applied pressure of 70 bar for 5 min.^{9,10} To ensure that the materials properties were comparable in the BL and NBL architectures, the BL cell was imprinted in an identical manner using a flat silicon wafer as the stamping-mold. A scanning electron microscopy (SEM) picture of the stamp is shown in Fig. 1(d). The stamp is produced by sputtering a 200 nm thick layer of aluminum on top of a silicon substrate before anodization at a constant voltage of 50 V in an oxalic acid solution of 0.3 molar at room temperature. A subsequent pore widening step in phosphoric acid (5 vol %) for 45 min produces pores with about 50 nm diameter and an average pore-to-pore distance of 100 nm.¹¹ After imprinting with the AAO stamp, the P3HT surface was analyzed by SEM [Fig. 1(e)]. For the lamination, PCBM (nano-C, 12 mg/ml in dichloromethane) was spin coated on mica at 1100 rpm for 30 s. The PCBM film was then lifted-off in a water bath and laminated on top of the P3HT film. Subsequently, the devices were placed in a glovebox, where a thin layer of LiF (about ~ 7 Å) and a 80 nm layer of Al were evaporated as a top contact.

Gracing incidence small angle x-ray scattering (GISAXS) was used to investigate the inner film structure.¹² The measurements were performed at beamline BW4 at HASYLAB (DESY, Hamburg). The wavelength was set to $\lambda=0.138$ nm and the sample detector distance to 1.99 m. The beam was adjusted to a size of $80 \times 40 \mu\text{m}^2$ by an assembly of beryllium lenses. In order to be well above the critical angle of the polymers the angle of incidence was $\alpha_i=0.363^\circ$.

Unlike the NBL device, the BL cell can be treated as a planar surface. As shown in Fig. 1(e), the nanostructured interface can be considered as an array of cylinders arranged on a planar surface. The cylinders have a feature-to-feature distance d , a radius r , and a height h . All of these values can be described by a distribution rather than a definite value. The average height and distance of the structures were obtained by fitting the GISAXS data simultaneously with a model based on the effective interface approximation and within the distorted wave Born approximation using the simulation software ISGISAXS.¹³ From these fits the obtained structural parameters are $d=80$ nm, $r=20$ nm, and $h=35$ nm. Based on these parameters, a surface increase factor z is calculated by

$$z = \frac{(2\pi r h + d^2)}{d^2},$$

resulting in an increase of 70% of interfacial surface area compared to a flat junction.

In order to determine whether the PCBM is able to fill the spaces between the P3HT pillars, GISAXS measurements were performed. Figure 2 shows the two-dimensional (2D) scattering images of the nanoimprinted P3HT film without (a) and with (b) a floated PCBM film on top. The prominent side maximum that is visible for the nanoimprinted P3HT film vanishes after coating the film. This can also be seen at the out-of-plane cuts in Fig. 2(c) taken at the critical angle of the polymer, which are additionally displayed together with the corresponding fits using an effective interface approximation, which is in good agreement with the fits obtained from ISGISAXS.¹⁴ As the refractive index of P3HT and PCBM are similar and that structures in the out-of-plane direction are not detectable, this is strong evidence that the PCBM

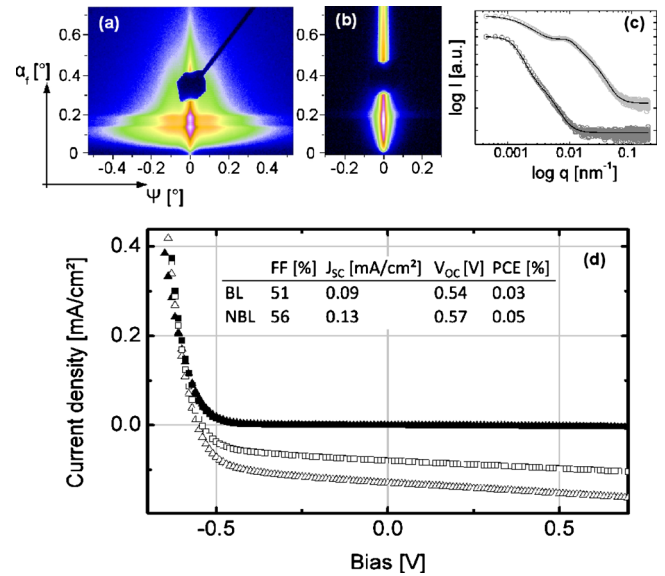


FIG. 2. (Color online) GISAXS scattering images of the nanoimprinted P3HT film without (a) and with (b) a coated PCBM film on top. The black square in the middle is the beamstop to shield the specular. The images were recorded using a Mar charge coupled device camera. (c) Double-logarithmic plot of out-of-plane cuts taken at the critical angle of P3HT (upper curve) and P3HT:PCBM (lower curve) films. The open symbols represent the experimental data and the solid lines the fit. For clarity the curves are shifted along the y-axis. The PCBM layer leads to a smooth surface topology and no more structures in out-of-plane direction are detectable after coating the P3HT with PCBM indicating a complete coverage of the P3HT. (d) I-V curve measured under simulated sunlight (AM1.5 g, 100 mW/cm²) of the NBL cell (open triangles) and BL cell (open squares), filled symbols show the respective dark curves.

layer covers the underlying nanostructure completely and leads to a smooth surface topology. Encapsulated pockets filled with possible residua such as water or air would lead to strong side features in the 2D scattering image.¹⁵

The SBL architecture has been developed in different laboratories over the past years.^{13,16,17} Orthogonal solvents were used in order to spin coat the PCBM layer on top of a P3HT layer [Fig. 1(b)]. In the case of P3HT and PCBM it is challenging to find good orthogonal solvents as they are originally designed and synthesized to show similar solving behavior. The best orthogonal solvent combination found was dichlorobenzene and dichloromethane. There are strong indications that this fabrication process does not lead to a BL configuration with an abrupt interface but rather to a continuous transition between P3HT and PCBM. For instance, these SBL solar cells show a short circuit current which is similar compared to a P3HT:PCBM blend solar cells. Furthermore, the incoming photon to current efficiency of the cells shows an increase when going from 50 to 80 nm thick P3HT films,¹⁷ which cannot be expected from a BL cell with an abrupt interface between PCBM and P3HT, for which an exciton diffusion length < 10 nm is reported.¹⁸

By measuring I-V curves under simulated solar radiation [Fig. 2(d)], an overall increase in current density of about 50% can be observed for the NBL cell compared with the BL cell, which is comparable to the increase in surface area (which is $\sim 70\%$). Beside an increase in current, an improvement of the open circuit voltage and the fill factor can also be seen, which leads to an overall improvement in the power conversion efficiency of about 80%.

Excitons with typical diffusion lengths of 10 nm (Ref. 19) and binding energies of 0.3 eV (Ref. 18) need to face an energetic discontinuity larger than their binding energy within their life time, otherwise they cannot contribute to the current. Using a rough estimation, there should be a direct linear dependency between the increased surface area and the increased current. Besides the mentioned mechanism, there are additional effects that might favor charge creation and/or transport, for instance a positive polymer alignment²⁰ in the pores, which might result in higher charge carrier mobility. Light trapping in nanostructured features could also be a positive factor. The effect of light trapping or scattering is likely a minor one because the absorption spectra indicate no significant difference between NBL and BL films.

However, there are also competing effects, such as higher recombination due to a higher surface area. Monte Carlo simulations²¹ show that the effective influence of the heterojunction angle, i.e., the angle of an organic–organic interface with respect to the contacts, is negligible, in the range of -90° to $+90^\circ$. This means that charge separation happening at the top of a nanopillar is approximately as efficient as separation at the side. However, in three-dimensional (3D)-morphologies with interfaces in a direction opposing the external field, the dissociation of electrons and holes creates an internal electric field pointing in the wrong direction leading to less efficient charge separation.²¹

In this respect nanowire structures might be ideal for efficient charge separation, better than 3D network structures. Thus the presented NBL cell architecture is interesting for further physical investigations, especially of physical processes at the interfaces. These well-defined nanostructured organic solar cells will allow to identify an ideal morphology. Further improvements can be expected by optimizing the film thicknesses of donor and acceptor material and decreasing the diameter and distance of the pillar structures down to the range of 10 nm and simultaneously increasing their height.

In summary, we present an organic solar cell with a network architecture in which there is direct control of the organic-organic interface morphology on a nanometer scale. Control over the morphology was made by a process of imprinting, followed by lamination. Our results show that orthogonal solvents do not supply the same abrupt interface. However, only clearly defined interfaces will allow a direct comparison of simulated results of nanostructured interfaces with experimental results, permitting the identification of ideal morphologies for organic solar cells.

We acknowledge the support by our CeNS partners, especially the groups of Professor Kotthaus and Professor Bein for access to their equipment (AFM, SEM). Furthermore, we would like to thank V. Körstgens, S. Roth, M. Rawolle, J. Perlich, and D. Magerl for the help during the GISAXS measurements. This work has been supported by the Deutsche Forschungsgemeinschaft (DFG) via the Cluster of Excellence EXC-4 “Nanosystems Initiative Munich (NIM)” and a DAAD/British Council grant.

¹G. Yu, J. Gao, J. C. Hummelen, F. Wudl, and A. J. Heeger, *Science* **270**, 1789 (1995).

²J. J. M. Halls, C. A. Walsh, N. C. Greenham, E. A. Marseglia, R. H. Friend, S. C. Moratti, and A. B. Holmes, *Nature (London)* **376**, 498 (1995).

³S. H. Park, A. Roy, S. Beaupre, S. Cho, N. Coates, J. S. Moon, D. Moses, M. Leclerc, K. Lee, and A. J. Heeger, *Nat. Photonics* **3**, 297 (2009).

⁴J. Y. Kim, K. Lee, N. E. Coates, D. Moses, T.-Q. Nguyen, M. Dante, and A. J. Heeger, *Science* **317**, 222 (2007).

⁵J. A. Barker, C. M. Ramsdale, and N. C. Greenham, *Phys. Rev. B* **67**, 075205 (2003).

⁶T. A. M. Ferenczi, J. Nelson, C. Belton, A. M. Ballantyne, M. Campoy-Quiles, F. M. Braun, and D. D. C. Bradley, *J. Phys.: Condens. Matter* **20**, 475203 (2008).

⁷L. C. Chen, D. Godovsky, O. Inganäs, J. C. Hummelen, R. A. J. Janssens, M. Svensson, and M. R. Andersson, *Adv. Mater.* **12**, 1367 (2000).

⁸For further informations please refer to: <http://www.obducat.com/>.

⁹Z. Song, B. H. You, J. Lee, and S. Park, *Microsyst. Technol.* **14**, 1593 (2008).

¹⁰G. Scarpa, A. Abdellah, A. Exner, S. Harrer, G. P. Blanco, W. Wiedemann, L. Schmidt-Mende, and P. Lugli, *IEEE Trans. Nanotechnol.* (to be published).

¹¹K. P. Musselman, G. J. Mulholland, A. P. Robinson, L. Schmidt-Mende, and J. L. MacManus-Driscoll, *Adv. Mater.* **20**, 4470 (2008).

¹²P. Müller-Buschbaum, *Anal. Bioanal. Chem.* **376**, 3 (2003).

¹³R. Lazzari, *J. Appl. Crystallogr.* **35**, 406 (2002).

¹⁴C. R. McNeill, A. Abrusci, I. Hwang, M. A. Ruderer, P. Müller-Buschbaum, and N. C. Greenham, *Adv. Funct. Mater.* **19**, 3103 (2009).

¹⁵G. Kaune, M. A. Ruderer, E. Metwalli, W. Wang, S. Couet, K. Schlage, R. Röhlberger, S. V. Roth, and P. Müller-Buschbaum, *ACS Appl. Mater. Interfaces* **1**, 353 (2009).

¹⁶C. J. Brabec, A. Cravino, D. Meissner, N. S. Sariciftci, M. T. Rispen, L. Sanchez, J. C. Hummelen, and T. Fromherz, *Thin Film Solids* **403–404**, 368 (2002).

¹⁷A. L. Ayzner, C. J. Tassone, S. H. Tolbert, and B. J. Schwartz, *J. Phys. Chem. C* **113**, 20050 (2009).

¹⁸O. V. Mikhnenko, F. Cordella, A. B. Sieval, J. C. Hummelen, P. W. M. Blom, and M. A. Loi, *J. Phys. Chem. B* **112**, 11601 (2008).

¹⁹J. E. Kroeze, T. J. Savenije, M. J. W. Vermeulen, and J. M. Warman, *J. Phys. Chem. B* **107**, 7696 (2003).

²⁰M. Aryal, K. Trivedi, and W. Hu, *ACS Nano* **3**, 3085 (2009).

²¹C. Groves, R. A. Marsh, and N. C. Greenham, *J. Chem. Phys.* **129**, 114903 (2008).